Journal of ELECTRONIC MATERIALS, Vol. 48, No. 5, 2019
https://doi.org/10.1007/s11664-019-06982-5

TOPICAL COLLECTION: 60TH ELECTRONIC MATERIALS CONFERENCE 2018

Photogalvanic Etching of *n*-GaN for Three-Dimensional Electronics

DANIEL M. DRYDEN ,[1,2,4] REBECCA J. NIKOLIC,[2] and M. SAIF ISLAM[3,5]

1.—Department of Materials Science and Engineering, University of California, Davis, Davis, CA, USA. 2.—Materials Engineering Division, Lawrence Livermore National Laboratory, Livermore, CA, USA. 3.—Department of Electrical and Computer Engineering, University of California, Davis, Davis, CA, USA. 4.—e-mail: dryden2@llnl.gov. 5.—e-mail: sislam@ucdavis.edu

Etching in wide-bandgap semiconductors such as GaN aids applications including transistors, sensors, and radioisotope batteries. Plasma-based etching can induce surface damage and contamination that is detrimental to device performance. We present a photoelectrochemical approach to etching *n*-type GaN (*n*-GaN) that is low-cost, simple, and environmentally benign compared to plasma approaches, with the potential for highly anisotropic etching that avoids material damage. *n*-GaN was etched in a dilute KOH solution with $K_2S_2O_8$ oxidizer, ultraviolet (UV) irradiation, and a catalytic metal mask which served as both photomask and counter electrode. Relatively smooth, highly anisotropic, non-defect-selective etching was achieved at rates in excess of 200 nm/min when etching at 65°C. The obstacle of bath acidification was circumvented using the addition of buffering salts to the etchant bath, substantially extending the etchant bath lifetime and etching depth achievable in a single, uninterrupted etch. These results represent a major step toward a scalable, device-ready electrochemical etch for vertical GaN structures and devices.

Key words: Gallium nitride, electrochemical etching, wide-bandgap semiconductors, semiconductor fabrication

INTRODUCTION

Micro- and nanostructured three-dimensional (3D) electronics find application across a broad array of devices, including power electronics,[1,2] optical sensors,[3] radiation detectors,[4–6] and radioisotope power sources.[7] Many of these applications further benefit from the use of wide-bandgap semiconductors such as gallium nitride (GaN), which has a large bandgap of 3.4 eV, high breakdown field, and a favorable figure of merit for high-frequency applications.[8] Defects introduced during etching, traditionally performed via plasma-based techniques,[9,10] are a limiting factor in the performance of vertical and quasi-vertical GaN devices.[1,10] GaN is impervious to many traditional wet etch chemistries,[11] and even those that work do not offer controllable anisotropy independent of planar orientation. There is thus a desire for a low-damage, high-anisotropy, patternable etch to facilitate next-generation 3D GaN electronics.

Photo-electrochemical (PEC) etching in its many varieties (Fig. 1) has shown promise as a means to address the aforementioned issues in GaN.[12–22] PEC etching avoids the damage inherent to physical plasma processes, exhibits controllable anisotropy, has excellent selectivity, and involves an experimental setup both simpler and less capital-intensive than plasma-based approaches. Alkaline etch chemistries further avoid the need for both toxic gases such as Cl_2 and SF_6, as well as avoiding the use of hydrofluoric acid.

The etching reaction of *n*-type GaN (*n*-GaN) in basic solution proceeds as follows:

(Received September 29, 2018; accepted January 18, 2019; published online January 31, 2019)

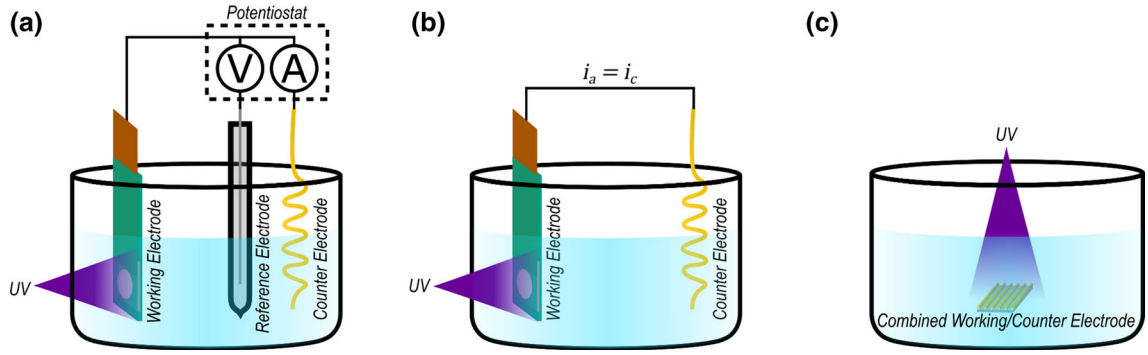

Fig. 1. Diagrams of photoelectrochemical etching experimental setups. (a) Photoelectrochemical etching with an external potentiostat and reference electrode, (b) photoelectrochemical etching at open-circuit potential, wherein the anodic and cathodic currents must be equal, and (c) photogalvanic etching.

$$GaN_{(s)} + 6OH^-_{(aq)} + 3h^+ \rightarrow GaO^{3-}_{3(aq)} + 3H_2O_{(l)} + \frac{1}{2}N_{2(g)} \quad (1)$$

Minsky et al.[12] first demonstrated the alkaline photo-etch of GaN, with the technique improved by Youtsey et al.[13] Bardwell et al.[14,15] demonstrated that a chemical oxidizer, $K_2S_2O_8$, could be added to the etching solution to increase the etching rate. The oxidizer is catalytically decomposed at the counter electrode surface and injects holes into the counter electrode metal:

$$S_2O^{2-}_{8(aq)} \rightarrow 2SO^{2-}_{4(aq)} + 2h^+ \quad (2)$$

The galvanic nature of the oxidizer's effect was later confirmed by Van Dorp et al.[16] Many experiments[16–20] used PEC as an external potentiostat to drive the etching reaction (Fig. 1a) both to create etched features and to elucidate the behavior of the etching system through electroanalytical experiments. The initial experiments,[12,13] however, were performed at open-circuit potential (Fig. 1b) with no external potentiostat, and Bardwell et al.'s[14,15] experimental setup used the still simpler photogalvanic approach (Fig. 1c).

In this photogalvanic configuration, the charge in the redox reaction is transferred directly between the working and counter electrode at the GaN-metal interface. The main benefit is the relative simplicity and ease of the etching process: the only external apparatus is the light source, and the counter electrode doubles as a photomask to define the etched features. This layout furthermore facilitates the etching of electrically isolated features: because the counter electrode is in electrical contact with the GaN anywhere the metal touches the surface, rather than at a single point as with an external counter electrode, the charge-balancing current is injected into the etched material evenly over the surface of the workpiece, even at isolated features to which no external electrode would be attached (e.g. pillars) in a traditional PEC etching setup. The primary drawback of the method is the limited counter electrode size: whereas an external electrode may be an arbitrary size, here the counter electrode area cannot be greater than the total surface area of the working electrode, and practical considerations (such as the dimensions of the features to be etched) often result in a substantially lower electrode area. This has the potential to limit the cathodic (counter electrode) current, which, given that the system is at open-circuit potential, must be equal to the anodic (etching) current. Care must therefore be taken to ensure that the counter electrode current is not the rate-limiting factor in the system, by e.g. increasing the concentration of oxidizer.

All aforementioned studies were performed on *n*-GaN, due not only to the relative availability and ease of manufacturing *n*-GaN versus *p*-type, but because *p*-type semiconductors tend to etch without ultraviolet (UV) illumination,[23] eliminating the mechanism by which etch features are photomasked and etch anisotropy is achieved. Within *n*-GaN, there is an inverse relationship between dopant density and etch rate[19] on account of the suppressed minority carrier lifetime with increased majority carrier concentration.

Previous work has demonstrated multi-micron deep etching, but has not commented on surface roughness,[13] or has demonstrated a smooth etch surface but only at limited depths and with severe trenching, or "reverse crown" profile, around etched features.[21] Furthermore, Maher et al.[22] observed that the $K_2S_2O_8$ oxidizer decomposes over time, acidifying the solution and limiting the etchant bath lifetime.

In this study, we explore the relationship between temperature, pH, bath stability, and etch quality in the system of alkaline photogalvanic etching of *n*-GaN. We demonstrate that etching quality can be substantially improved by gently heating the etching solution, and furthermore demonstrate a substantial increase in etchant lifetime and pH stabilization through the use of a buffered etch solution consisting of phosphate salts that

counteract the pH change caused by $K_2S_2O_8$ decomposition. With this system, we demonstrate control over the 5-μm-deep anisotropic etching of three-dimensional, micron-scale GaN features.

EXPERIMENTAL

Samples consisted of c-face n-GaN on sapphire with a nominal GaN thickness of 5 μm or 10 μm, and nominal carrier concentration of 1e19 cm^{-3} or 8e16 cm^{-3}, respectively. The galvanic contact was deposited via electron beam deposition and patterned via standard liftoff lithography. The metal contact was comprised of 300-Å Ti, 710-Å Al, 500-Å Pt, and 1000-Å Au, a contact composition providing a stable, low-work function interface and a noble metal surface.[24] The contact covered approximately 17% of the surface, or a 5:1 GaN-to-metal surface area ratio. The contact was not annealed and showed ohmic conduction. The substrate was cleaned using O_2 plasma and buffered HF before contact deposition.

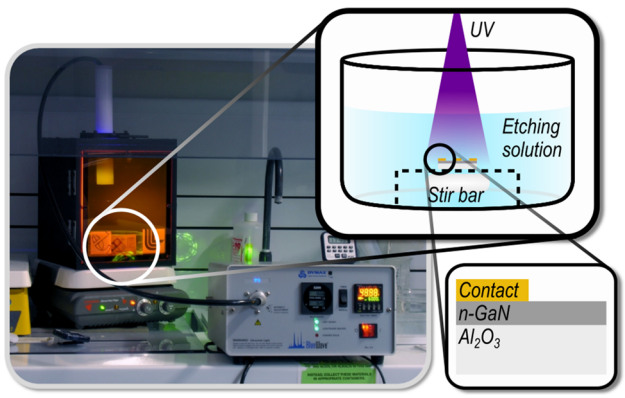

Fig. 2. Left: Picture of experimental apparatus. Right: Diagram of etchant bath with UV light and stirrer (top) and schematic of the n-GaN sample and metal contact (bottom).

Samples were etched using the setup shown in Fig. 2, consisting of a Dymax Bluewave75 Xe lamp (Dymax, Inc.), an UV-tight enclosure, an etchant bath, and a hotplate/stirrer. The etchant bath consisted of 200 mL of 0–25 mM KOH, 0–150 mM Na_3PO_4 (phosphate salt tribasic), and 0–150 mM $K_2S_2O_8$ in DI water. The illumination intensity was approximately 120 mW/cm^2 for $\lambda < 365$ nm as measured by UV radiometer on all samples unless otherwise noted. Samples were characterized using a Hitachi S-800 scanning electron microscope (SEM; Hitachi, Ltd.) and an AFM Workshop TT-2 atomic force microscope (AFM; AFM Workshop, USA).

RESULTS

Samples of n-GaN with a nominal carrier concentration of 10^{19} cm^{-3} etched at room temperature (Fig. 3a) showed a very slow etch rate, with smooth etching near the metal contacts and surface roughening elsewhere. This surface roughening can be attributed to a defect-selective etching regime, in which the areas around defect centers are not removed due to their electronically active trap states.[25] Increasing the temperature to 65°C results in an increase in both etching rate and etching quality (Fig. 3b). From cross-sectional SEM images, the etch rate near the galvanic contacts was 70 nm/min, decreasing with distance from the contacts, resulting in trenching near the metal contacts and a "reverse crown" profile typical of diffusion-limited etches.[21]

Others have reported the acidification of the etchant bath with UV exposure,[22] via breakdown of the $K_2S_2O_8$ oxidizer. Figure 4 shows the progression of bath pH over time at room temperature and 65°C, with and without the addition of buffering salts. The acidification is measurable at room temperature, but accelerates dramatically at elevated temperature, rapidly acidifying after 20 min at 65°C. Increasing the etching time to 60 min resulted in the formation of a thick, cracked oxide

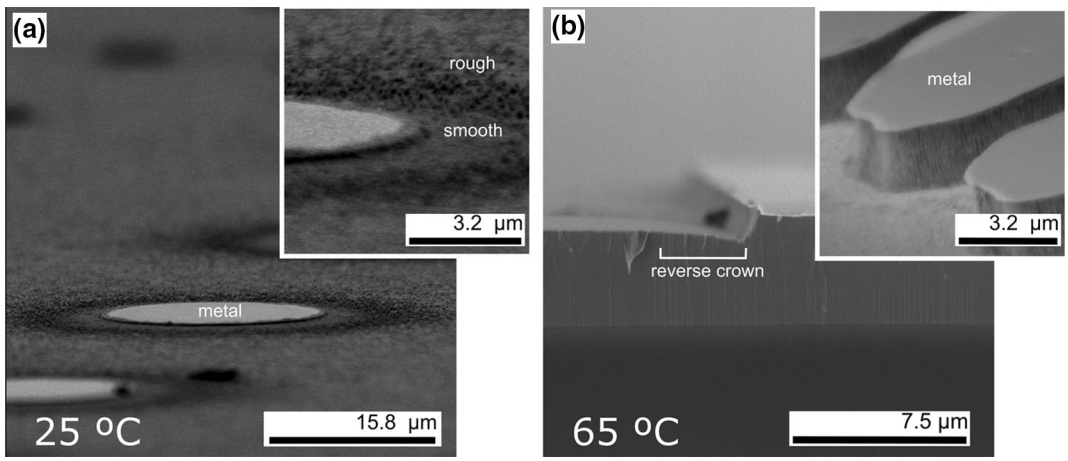

Fig. 3. (a) Sample etched in 25 mM KOH/150 mM $K_2S_2O_8$ and 115 mW/cm^2 UV light for 20 min, unstirred, at ambient temperature. Inset: closeup of etched feature edge. (b) Sample etched under identical conditions to (a) but heated to 65°C. Inset: closeup of etched feature sidewall.

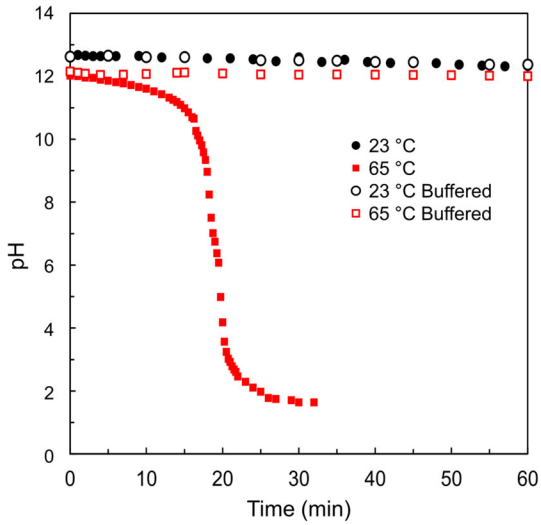

Fig. 4. Change in etchant bath pH under UV irradiation with time. At room temperature (black), the unbuffered (filled) and buffered (unfilled) symbols overlay one another. At 65°C (red), the unbuffered solution rapidly acidifies over 20 min while the buffered solution remains relatively stable (Color figure online).

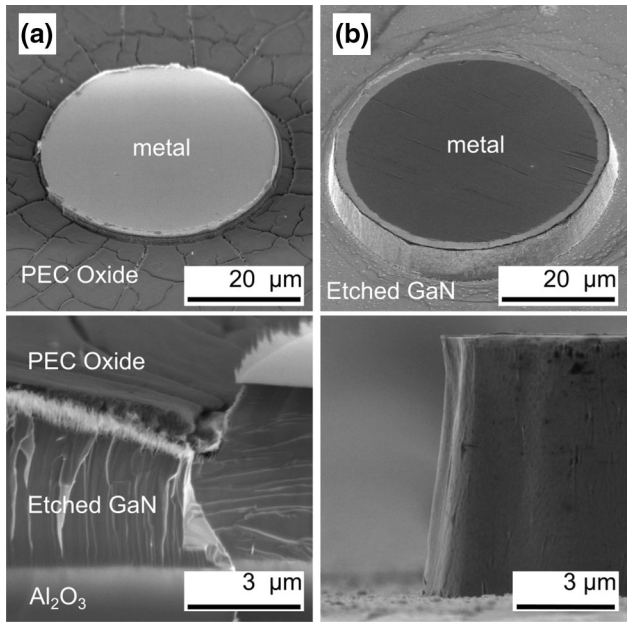

Fig. 5. (a) SEM micrograph of GaN etched for 60 min in unbuffered solution: top view (upper) and in cross section (lower). (b) GaN etched for 30 min in buffered solution: top view (upper) and section view (lower).

layer on top of the etched material (Fig. 5a). The acidification was remedied by the addition of 150 mM Na_3PO_4 buffering salt which stabilized the solution above pH 12, within the alkaline etching regime of GaN.[26,27] A 30-min etch on unintentionally doped n-GaN with a nominal carrier concentration of 8×10^{16} cm^{-3} (Fig. 5b) with the buffered solution removed approximately 7 μm of material, a rate of 233 nm/min, without the formation of insoluble oxide. The resulting features had sidewall angles between 80° and 83°, and the horizontal etched surfaces had a root-mean-squared roughness of 24 nm, versus 4.9 nm for the unetched GaN.

DISCUSSION

The PEC etching mechanism relies on multiple simultaneous processes, any of which may be rate-limiting depending on the etching conditions. The etching morphology is particularly sensitive to the balance between the flux of OH^- ions in solution and the flux of h^+ within the GaN to the GaN-electrolyte interface. If the h^+ are the limiting reagent (KOH is in excess), etching will only occur where h^+ are able to reach the etching interface; within a certain radius of h^+-trapping defects such as threading dislocations, there will not be sufficient h^+ to drive the etching reaction, and the material will etch in the defect-selective regime.[25] This can be seen in the bumps visible on the etched surface in Fig. 3a, where h^+ near dislocation cores are trapped in defect states rather than contributing to the etching reaction, resulting in features that either do not etch or etch more slowly than the non-defective GaN.[25] Under conditions where h^+ are in excess, the etching process will be limited by the mass transfer of OH^- to the etching surface. With an excess of h^+ wherever the OH^- ions reach the surface, the material will etch in the defect-nonselective regime at a rate proportional to the local flux of OH^-. This regime is evident in Fig. 3b, where etching is smooth everywhere but enhanced near metal contacts, above which the KOH is not depleted by local etching. This higher concentration of KOH near the metal contacts results in a steeper concentration gradient of KOH to the surface, and thus faster etching. This trenching, or "reverse crown" profile, is the result of an unstirred solution, in which the KOH diffusion layer extends well beyond the etching depth in the region above exposed GaN; in Fig. 5b, wherein the etching solution was stirred for the first 20 min of the etch, the trenching is largely absent.

The rate of KOH flux can be controlled by changing solution pH, stirring the solution, or changing the etching temperature. An increased temperature not only increases the rate of KOH diffusion to the surface but results in convection mixing as well. The rate of h^+ flux is affected by considerably more variables: the rate of h^+ generation is dependent on UV illumination intensity; the h^+ lifetime is sensitive to defect density and dopant concentration, the latter also controlling the surface depletion region depth and thus the volume of material in which generated h^+ may be effectively separated from their accompanying e^- without undergoing recombination[28] (This dependence of h^+ generation rate on depletion region width, and thus on the material's carrier concentration, is likely responsible in part for the marked difference in etch rate between the highly doped material

shown in Fig. 3b and the lower-doped material in Fig. 5b). Furthermore, the photo-generated e^- must be consumed by a counter electrode (reduction) half-reaction to provide charge balance and allow for the continued separation of h^+. This rate is dependent on the mass transfer of $K_2S_2O_8$ in solution to the metal contact surface, which is controlled by the same factors as the KOH flux, namely, concentration, mixing, and temperature. The catalytic reduction of $K_2S_2O_8$ injects h^+ into the metallic contact, which diffuse to the metal-GaN contact and recombine with conduction band e^-; the rate of this charge diffusion and recombination also affect the h^+ flux to the etching interface.

All the aforementioned rates are expected to have a temperature dependence, and an increase in temperature does not uniformly favor the defect-selective or defect-nonselective regime across all affected rates. It is therefore difficult to accurately predict the effect varying temperature will have on the etching process. Empirically, however, the results shown in Fig. 3 demonstrate that a modest increase in etching bath temperature from room temperature to 65°C not only increases the etching rate but also tends to favor defect-nonselective etching as well. Experiments are ongoing to investigate the effect of solution mixing and GaN-metal interface charge transport to more fully understand the role each mechanism plays in the etching process, and to further optimize etching conditions.

Solution acidification has been attributed primarily to the decomposition of $K_2S_2O_8$ into sulfuric and monopersulfuric acid[22] by both UV photolysis[29] and thermal decomposition.[30] The acidification is slow but measurable at room temperature, but considerably accelerated at 65°C (Fig. 4). The breakdown of $K_2S_2O_8$ not only prevents the oxidizer from effectively maintaining charge balance as intended, but shifts the etching bath pH to a regime where the oxidation of GaN does not produce soluble gallates, but instead produces insoluble Ga_2O_3 or mixed oxide-hydroxides.[26,27] Sources differ[26,27,31,32] as to the pH threshold below which Ga oxidizes into insoluble compounds; calculated Pourbaix diagrams are sensitive to the method of calculation, source of thermodynamic data, and concentration and presence of species assumed to be present.[26,33] This pH threshold, the compounds present above and below it, and the etching conditions in its vicinity are all fruitful subjects for further research. Solutions above pH 12 are generally shown to be effective in creating soluble gallates as the oxidation products of GaN. Therefore, Na_3PO_4 was chosen as a buffering salt to stabilize the solution pH. The PO_4^{3-} ion has a pKa of 12.3, indicating that below a pH of 12.3 the ion will tend to bind to H^+:

$$PO^{3-}_{4(aq)} + H^+_{(aq)} \rightarrow HPO^{2-}_{4(aq)}, \quad pKa = 12.3 \qquad (3)$$

As the breakdown of $K_2S_2O_8$ generates free H^+, the PO_4^{3-} ions in solution scavenge them, slowing the solution acidification and stabilizing the pH. The addition of the buffering salts creates a bath that has a substantially longer functional lifetime than previously reported unbuffered alkaline chemistries. This longer lifetime facilitates etching at elevated temperatures, which improves the surface quality of the etch and reduces defect selectivity; the longer bath life also eases deep etching, which can be achieved in a one-pot setup rather than having to constantly replenish or replace the etchant bath. Further experiments are ongoing to explore the effect of buffer concentration and pH on GaN etching rate and morphology.

CONCLUSION

Photogalvanic etching of *n*-GaN in alkaline solutions has been demonstrated as an effective way to achieve smooth, deep, high-anisotropy features using a simple, one-pot reaction that avoids the use of HF or toxic gases. From experiments run at temperatures from 23°C to 65°C, the presented unbuffered etching conditions were achieved at 65°C in an unstirred solution of 25 mM KOH (pH 12.4) and 150 mM $K_2S_2O_8$ in DI water with 120-mW/cm^2 UV irradiation. The buffered conditions were identical, save for the addition of 150 mM Na_3PO_4 buffering salt (pH 12.78). Deep etching was achieved by etching at elevated temperatures and counteracting bath acidification with the use of phosphate buffering salts in the etching solution, substantially extending the lifetime of the etchant bath and facilitating deep, anisotropic etching. Work is ongoing to improve surface morphology and explore the mechanisms by which temperature, pH, and other factors affect the etch process.

ACKNOWLEDGMENTS

This work was performed under the auspices of the U.S. Department of Energy by Lawrence Livermore National Laboratory under contract no. DE-AC52-07NA27344, LLNL-JRNL-758918. The authors would like to thank the following sources of funding: Army Research Office (ARO-W911NF-14-4-0341) and the LLNL Livermore Graduate Scholar Program.

REFERENCES

1. Y. Zhang, A. Dadgar, and T. Palacios, *J. Phys. Appl. Phys.* 51, 273001 (2018).
2. J. Millan, P. Godignon, X. Perpina, A. Perez-Tomas, and J. Rebollo, *IEEE Trans. Power Electron.* 29, 2155 (2014).
3. Y. Gao, H. Cansizoglu, K.G. Polat, S. Ghandiparsi, A. Kaya, H.H. Mamtaz, A.S. Mayet, Y. Wang, X. Zhang, T. Yamada, E.P. Devine, A.F. Elrefaie, S.-Y. Wang, and M.S. Islam, *Nat. Photonics* 11, 301 (2017).
4. A.M. Conway, T.F. Wang, N. Deo, C.L. Cheung, and R.J. Nikolic, *IEEE Trans. Nucl. Sci.* 56, 2802 (2009).
5. D.S. McGregor, S.L. Bellinger, and J.K. Shultis, *J. Cryst. Growth* 379, 99 (2013).

6. Q. Shao, L.F. Voss, A.M. Conway, R.J. Nikolic, M.A. Dar, and C.L. Cheung, *Appl. Phys. Lett.* 102, 063505 (2013).
7. M.A. Prelas, C.L. Weaver, M.L. Watermann, E.D. Lukosi, R.J. Schott, and D.A. Wisniewski, *Prog. Nucl. Energy* 75, 117 (2014).
8. F. Medjdoub and K. Iniewski, *Gallium Nitride (GaN): Physics, Devices and Technology* (2016).
9. S.E. Harrison, L.F. Voss, A.M. Torres, C.D. Frye, Q. Shao, and R.J. Nikolić, *J. Vac. Sci. Technol. Vac. Surf. Films* 35, 061303 (2017).
10. Y. Zhang, M. Sun, H.Y. Wong, Y. Lin, P. Srivastava, C. Hatem, M. Azize, D. Piedra, L. Yu, T. Sumitomo, N.A. de Braga, R.V. Mickevicius, and T. Palacios, *IEEE Trans. Electron Devices* 62, 2155 (2015).
11. D. Zhuang and J.H. Edgar, *Mater. Sci. Eng. R Rep.* 48, 1 (2005).
12. M.S. Minsky, M. White, and E.L. Hu, *Appl. Phys. Lett.* 68, 1531 (1996).
13. C. Youtsey, I. Adesida, and G. Bulman, *Appl. Phys. Lett.* 71, 2151 (1997).
14. J.A. Bardwell, I.G. Foulds, J.B. Webb, H. Tang, J. Fraser, S. Moisa, and S.J. Rolfe, *J. Electron. Mater.* 28, L24 (1999).
15. J.A. Bardwell, J.B. Webb, H. Tang, J. Fraser, and S. Moisa, *J. Appl. Phys.* 89, 4142 (2001).
16. D.H. van Dorp, J.L. Weyher, M.R. Kooijman, and J.J. Kelly, *J. Electrochem. Soc.* 156, D371 (2009).
17. G. Nowak, X.H. Xia, J.J. Kelly, J.L. Weyher, and S. Porowski, *J. Cryst. Growth* 222, 735 (2001).
18. B. Yang and P. Fay, *J. Vac. Sci. Technol. B Microelectron. Nanometer Struct.* 22, 1750 (2004).
19. L. Macht, J.J. Kelly, J.L. Weyher, A. Grzegorczyk, and P.K. Larsen, *J. Cryst. Growth* 273, 347 (2005).
20. K. Al-Heuseen, M.R. Hashim, and N.K. Ali, *Appl. Surf. Sci.* 257, 6197 (2011).
21. J.L. Weyher, F.D. Tichelaar, D.H. van Dorp, J.J. Kelly, and A. Khachapuridze, *J. Cryst. Growth* 312, 2607 (2010).
22. H. Maher, D.W. DiSanto, G. Soerensen, C.R. Bolognesi, H. Tang, and J.B. Webb, *Appl. Phys. Lett.* 77, 3833 (2000).
23. J.L. Weyher and J.J. Kelly, in *Springer Handbook Crystal Growth* (Springer, Berlin, Heidelberg, 2010), pp. 1453–1476.
24. G. Greco, F. Iucolano, and F. Roccaforte, *Appl. Surf. Sci.* 383, 324 (2016).
25. J.L. Weyher, L. Macht, F.D. Tichelaar, H.W. Zandbergen, P.R. Hageman, and P.K. Larsen, *Mater. Sci. Eng., B* 91–92, 280 (2002).
26. N. Takeno, *Atlas of Eh-PH Diagrams* (National Institute of Advanced Industrial Science and Technology Research Center for Deep Geological Environments, 2005).
27. B.L. Pearce, S.J. Wilkins, T. Paskova, and A. Ivanisevic, *J. Mater. Res.* 30, 2859 (2015).
28. J.L. Weyher, D.H. van Dorp, and J.J. Kelly, *J. Cryst. Growth* 430, 21 (2015).
29. L. Dogliotti and E. Hayon, *J. Phys. Chem.* 71, 2511 (1967).
30. I.M. Kolthoff and I.K. Miller, *J. Am. Chem. Soc.* 73, 3055 (1951).
31. J. Price, J. Barnett, S. Raghavan, M. Keswani, and R. Govindarajan, *Microelectron. Eng.* 87, 1661 (2010).
32. B. Swain, C. Mishra, L. Kang, K.-S. Park, C.G. Lee, and H.S. Hong, *Environ. Res.* 138, 401 (2015).
33. H.-H. Huang, *Metals* 6, 23 (2016).